Emergent Materials (2023) 6:1167–1176
https://doi.org/10.1007/s42247-023-00503-1

ORIGINAL ARTICLE

Nitrogen and sulfur co-doped activated carbon nanosheets for high-performance coin cell supercapacitor device with outstanding cycle stability

Susmitha Uppugalla[1] · Ramyakrishna Pothu[2] · Rajender Boddula[3] · Mangesh A. Desai[4] · Noora Al-Qahtani[3]

Received: 31 January 2023 / Accepted: 3 May 2023 / Published online: 15 May 2023

Abstract

Herein, we report the utilization of nitrogen and sulfur dual heteroatoms co-doped activated carbon (NSAC) by hydrothermal method for electrochemical supercapacitors. Various NSACs were made by using a fixed amount of activated carbon and changing the amounts of thioacetamide. From NSAC electrodes, the coin cell configuration was fabricated and the overall electrochemical conduct was evaluated by using cyclic voltammetry, galvanostatic charge-discharge, cycle life, and electrochemical impedance methodologies. The outcomes manifest that co-doping sulfur and nitrogen into the AC improves the electrochemical performance. In comparison to pure activated carbon, the optimized NSAC produced a higher specific capacitance value of 417 F g^{-1} at 0.7 A g^{-1} and also demonstrated outstanding charge-discharge cycling stability at 7 mA (5 A g^{-1}), maintaining 76% of its opening capacitance after 60,000 cycles in the CR2032 device configuration. The impedance studies phase angle value of 85° has added evidence of the NSAC's good capacitor performance. Thus, we believe this work is suitable for practical applications for energy storage devices.

Keywords Activated carbon · Hydrothermal synthesis · Heteroatom-doped carbon · Supercapacitor · Self-discharge · Leakage current

1 Introduction

In recent years, human civilization has regularly encountered expanding energy needs and environmental pollution that are a result of global changes. In order to mitigate issues like air pollution, acid rain, and the greenhouse effect, it is imperative to build cutting-edge, eco-friendly renewable energy storage systems and rely less on fossil fuels [1–4]. The coming years of energy calamity due to the depletion of fossil fuels are urgently sound for the economic, effectual, and sustainable energy conversion and energy storage technologies to face the

Highlights
- Hydrothermal strategy for heteroatom-doped activated carbon.
- Fabrication of symmetric supercapacitor cell using coin cell device assembly.
- NSAC exhibits an excellent capacitance, energy density, and power density of 336 F g^{-1}, 57 W h kg^{-1}, and 5500 W kg^{-1} at 5 A g^{-1}.
- Symmetric coin cell device exhibits an excellent energy density of 70 W h kg^{-1}.
- Exceptional capacity retention of more than 76% was achieved after more than 60,000 cycles at 5 A g^{-1}.

✉ Susmitha Uppugalla
susmitha.uppugalla@gmail.com

✉ Rajender Boddula
research.raaj@gmail.com

✉ Noora Al-Qahtani
noora.alqahtani@qu.edu.qa

Ramyakrishna Pothu
research.ramyakrishna@gmail.com

Mangesh A. Desai
drmangesh6@gmail.com

[1] Bio Enviro Chemical Solutions, 530017 Visakhapatnam, India

[2] School of Physics and Electronics, College of Chemistry and Chemical Engineering, Hunan University, Changsha 410082, P.R. China

[3] Center for Advanced Materials (CAM), Qatar University, 2713 Doha, Qatar

[4] Admatius Innovations Pvt. Ltd., Pune 411057, India

matter of escalating energy requirements. When considering the various options for storing energy, supercapacitors, which have a higher power density and are more environmentally friendly than secondary batteries, are widely used in a variety of manufacturing processes, battery-powered hybrids, and portable electronics [5]. Supercapacitors are energy storage devices and are separated into two major categories based on the operation of energy storage, electric double layer capacitors (EDLC) engaging carbon-based materials and pseudocapacitors (PC) employing conducting polymers and metal oxides active electrode materials [6]. EDLC is the most dominating charge storage mechanism in the case of supercapacitors which occurs over the surface of the electrode material. Thus, high activity and wettability of the electrode material are badly demanded. PCs have high capacitances associated with faradic redox processes; however, they suffer from a slow charge-discharge rate and poor cycling stability. Because in PCs, the redox reactions are not fully reversible and also suffer from material degradation due to the expansion-contraction of the electrodes, poor electrical conductivity, and high cost, limiting their further applications [7]. Compared with PCs, EDLCs have superior cycling stability and lower cost. Thus, carbon-containing materials (activated carbons, carbon nanotubes, carbon fibers, and graphene) are utilized as active electrodes for EDLC applications due to their high electrical conductivity, large surface area, strong chemical stability, and availability [6, 8, 9].

Nanocarbon materials have been used for several applications such as sensing, catalysis, energy storage, and water purification due to their extraordinary physico–chemical properties. Among several nanocarbons, activated carbon (AC) is one of the most exploited materials for the above-mentioned applications. The recent struggles in the development and research of electrochemical supercapacitors are mostly focused on accomplishing high-specific energy and power with prolonged life. However, for industrialization, low-cost electrode materials are highly demanded, wherein activated carbon fits well. In order to use carbon materials for practical energy storage applications, they have been doped with heteroatoms such as nitrogen (N) and sulfur (S); as a result, such materials delivered improved electrochemical performance. Additionally, a few reports mentioning carbon doping with boron, oxygen, phosphorus, etc. are also regularly found. Heteroatoms eliminate the electroneutrality of carbon materials because their heteroatoms have lower (B, P) or higher (N, O) electronegativity than carbon [10] and pseudocapacitance effect originating from electron donor/acceptor properties of heteroatoms [11]. On the other hand, the substitutional doping of nitrogen has been popular because of important changes in the hardness and chemical reactivity of carbon materials which is theoretically predicted and experimentally observed [12]. The π-system of the C lattice and N lone-pair conjugation can significantly affect or advance the physicochemical properties of the ACs, such as the basicity, catalytic activity, conductivity, and oxidative stability [13]. The increased capacitance brought on by N-doping was thought to be mostly caused by nitrogen functions, especially N, which exhibits pseudocapacitive behavior and an electron donor propensity [14]. Despite that, it is intriguing to understand that co-doping can lift up the performance of the electrode materials in comparison with single heteroatom-doped electrode materials. Additionally, co-doping can produce several positive effects such as improvement in conductivity and surface area of the electrode material. As a result, electrochemical charge storage properties can be boosted; thus, in recent days, efforts have been concentrated on the utilization of multi-heteroatom doping [15]. Through redox processes, heteroatoms other than N, such as B, P, or S atoms, also contribute to the amplification of capacitance in carbon-based materials. Due to the N- and S-dopant's synergistic interaction and possible easier polarizability, sulfur, in particular, is of great interest. Recent research has concentrated on using sulfur-doped carbons in supercapacitors [16]. Because sulfur transforms the charge on nearby carbon atoms to a more positive state in sulfuric acid, the efficiency of charge storage in microscopic pores via EDLC is improved. S-doped carbons were demonstrated; photoactivity and potential cycling have been found to greatly enhance the capacitance in both neutral and acidic electrolytes [16–19]. The objective of this work is to enhance the electrochemical capacitive performance of AC by incorporating hetero atoms (nitrogen and sulfur doping) into it. Nitrogen and sulfur co-doped activated carbons (NSACs) offer uniform distribution and controlled incorporation of heteroatoms all over the material compared to the post-treatment methods which are laborious and complex.

2 Experimental

2.1 Materials and instrumentation

Activated carbon (purchased from Merck), thioacetamide (C_2H_5NS), sulfuric acid (H_2SO_4) [Rankem, India], Super-P carbon black, and PVDF. All the reactions were carried out with distilled water.

FT-IR spectra of carbon samples carried with KBr pellet method by FT-IR spectrometer (Thermo Nicolet Nexus 670, USA). A Hitachi S-4300 SE/N field emission scanning electron microscope (FESEM) (Hitachi, Tokyo, Japan) running at 20 kV was used to conduct morphology analyses on the carbon samples. The elemental analysis (C, H, N, and S) was performed by the instrument (Vario Micro Cube Elementar, Germany). Micro-Raman spectra were carried out with a 17 mW internal He-Ne (Helium-Neon) laser source with an

excitation wavelength of 632.8 nm at room temperature, which is built into the Horiba Jobin-Yvon Lab Ram HR spectrometer. At room temperature, supercapacitor cells were used for all electrochemical tests. Using a ZIVE MP5 multichannel electrochemical workstation, cyclic voltammetry and galvanostatic charge-discharge cycle life studies were performed (WonATech Co., Ltd., Korea). A supercapacitor cell was used for the electrochemical impedance spectroscopy (EIS) measurement with an IM6ex (Zahner-Elektrik, Germany) at a DC bias of 0 V and a sinusoidal signal with an amplitude of 10 mV spanning the frequency range of 40 kHz to 10 mHz.

2.2 Synthesis of nitrogen and sulfur-doped activated carbons

Three various N- and S-doped activated carbons were prepared by hydrothermal synthesis using fixed amounts of activated carbon (AC) and various amounts of thioacetamide (C_2H_5NS). A typical technique involved dispersing 0.3 g of AC in 100 ml of water using a sonicator for 30 min, followed by the addition of a certain quantity of C_2H_5NS dissolved in 60 ml of water and a 5-min stirring period. The resulting mixture was shifted into a stainless steel autoclave with a volume of 250 mL, and it was hydrothermally treated at 180 °C overnight. After that, we allowed cooling naturally to ambient temperature to collect the resultant black product after cleaning with distilled water and acetone to get rid of any remaining unreacted substances. The sample was then dried for additional characterization in an oven at 60 °C. Compared to the AC, an excessive amount of C_2H_5NS was added to the experiment. The C_2H_5NS to activated carbon ratios were 2.5, 5, and 10. The related activated carbons with nitrogen and sulfur doping were designated as NSAC-1, NSAC-2, and NSAC-3, respectively. The pristine sample of activated carbon (where C_2H_5NS was not used) is named as hydrothermal-treated activated carbon (HTAC).

2.3 Construction supercapacitor cell

Coin cell (CR2032) supercapacitor was built with two working electrodes of equal mass separated by an AGM separator in an electrolyte of 1 M H_2SO_4. The working electrode is prepared by a 3 mg carbon sample composed of 70 wt.% active material (2.1 mg), 5 wt. % Super-P carbon black (0.15 mg), and 25 wt.% PVDF binder (0.75 mg) by applying pressure of 120 kg cm^2 to carbon samples placed on stainless steel mesh (316 grade); working electrodes were created.

3 Results and discussion

The intention of this research is to enhance the supercapacitor's carbon electrode's performance through the doping of heteroatoms. Three different samples of carbon powder doped with heteroatoms were prepared by reacting activated carbon with various amounts of C_2H_5NS for optimization in the autoclave.

Herein, thioacetamide is the nitrogen and sulfur heteroatoms precursor. The CHNS elemental analysis exhibited the presence of 3.09, 5.23, and 8.17 wt. % N and 3.06, 4.73, and 5.19 wt. % S for NSAC-1, NSAC-2, and NSAC-3 samples correspondingly. These heteroatoms can significantly increase the surface activity when they can tune the physical and chemical properties of carbon atoms such as increment in the conductivity and enhanced capacitance due to the conjugation between the π-system of the carbon framework and the lone-pair electrons of heteroatoms. For further confirmation of the elemental (i.e., nitrogen and sulfur especially) and compositional analysis, we have carried out X-ray photoelectron spectroscopy (XPS) studies.

Figure 1 demonstrates core level XPS spectra of the HTAC (Fig. 1a–c) and NSAC-2 (Fig. 1d–f) samples. The C 1s peak at 284.5 eV was present for both the samples, as illustrated in Fig. 1a (HTAC) and Fig. 1c (NSAC-2) which was attributed to the sp^2 hybridized carbon atom (peak C_1). Additionally, two other peaks were observed at binding energies from 285.0 to 291.0 eV, which were assigned to oxygen and/or sulfur-nitrogen-bound carbon atoms (peaks C_2 and C_3). In HTAC samples, the absence of sulfur and nitrogen was seen (Fig. 1b,c). The nitrogen doping in NSAC-2 samples (Fig. 1e) was confirmed, and four peaks (N_1 to N_4) were fitted during the deconvolution. The occurrence of pyridinic, pyrrolic, and quaternary nitrogen atoms within the carbon framework may give rise to such peaks [20]. The core level XPS spectra of sulfur 2P of NSAC-2 samples (Fig. 1f) confirm S-doping. The deconvolution (S_3 and S_4) suggested that oxidized S species, such as sulfate and sulfonate functional groups, lead to a peak at 168.8–172 eV. On the other hand, spin-orbit splitting of S atoms (S_1 and S_2) was noted within the range of 163–166 eV due to the formation of S dominated in the carbon framework [21].

The XRD patterns (Fig. 2a) seen in both HTAC and NSAC samples demonstrate broad diffraction peaks which reveals a predominantly amorphous structure. Previously, it has been proven that such an amorphous nature is attributed to high surface area and can provide excellent electrochemical properties. However, two distinct diffraction peaks were observed at 23.2° and 44.3° in each sample corresponding to the disordered carbon (001) and (100) crystalline planes, which were in accordance with JCPDS No. 41-1487 [22]. FT-IR analysis verified the functional groups on the prepared carbon samples (Fig. 2b). The -O-H and -N-H stretching vibration modes were connected to the broad bands at about 3450 cm^{-1}. The C-H bond is represented by the weak band at roughly 2920 cm^{-1}, and the characteristic absorbance of C-H bonds is represented by the band at about 1600 cm^{-1}. The presence of the C-N stretching vibration may be

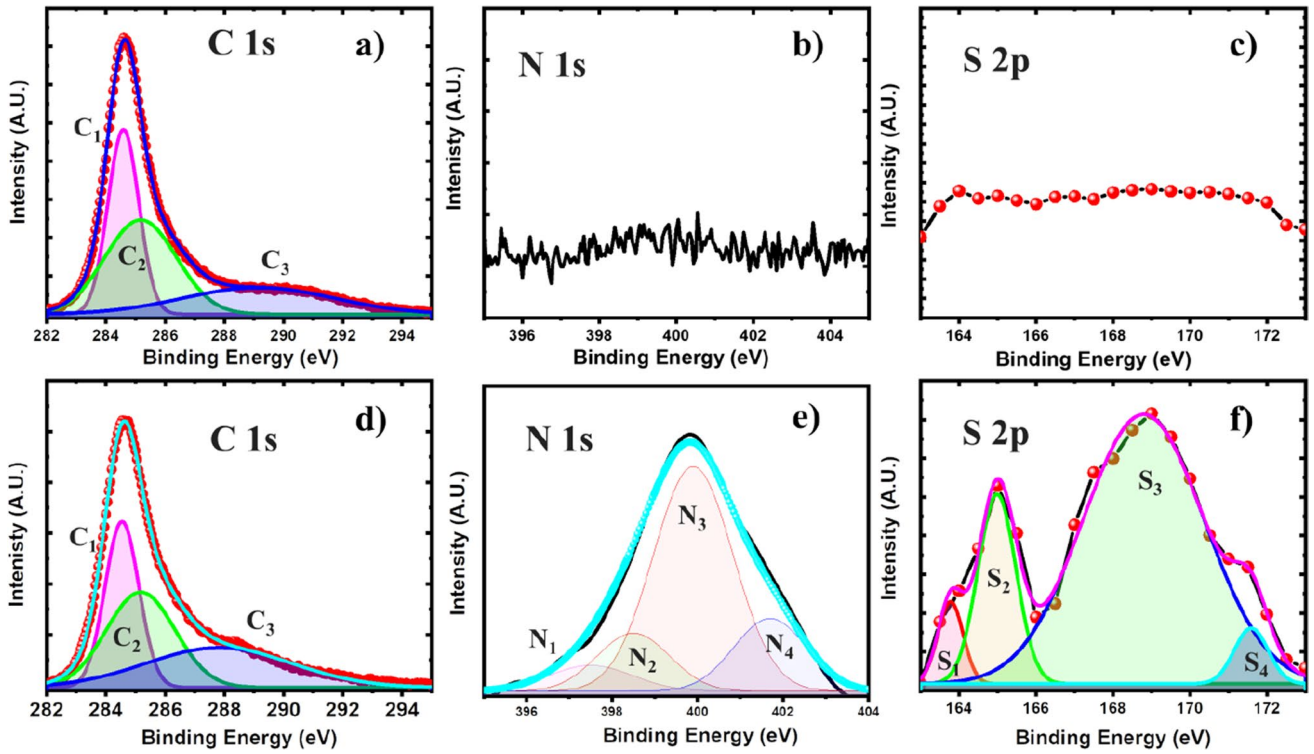

Fig. 1 Core level XPS spectra of the HTAC (**a**–**c**) and NSAC-2 (**d**–**f**) samples: (**a**, **d**) carbon 1S, (**b**, **e**) nitrogen 1S, and (**c**, **f**) sulfur 2P

inferred from the peaks at about 1130 cm^{-1}. The increase in the intensity of the band at 1125 cm^{-1} is remarkable; as in this spectral region, the υ(C = S) and υ(S = 0) vibrations occur. The wide peak of 1100 cm^{-1} is linked to the vibration of C-N stretching. With an increase in sulfur content, the water absorption band around 1650–1885 cm^{-1} of carbons

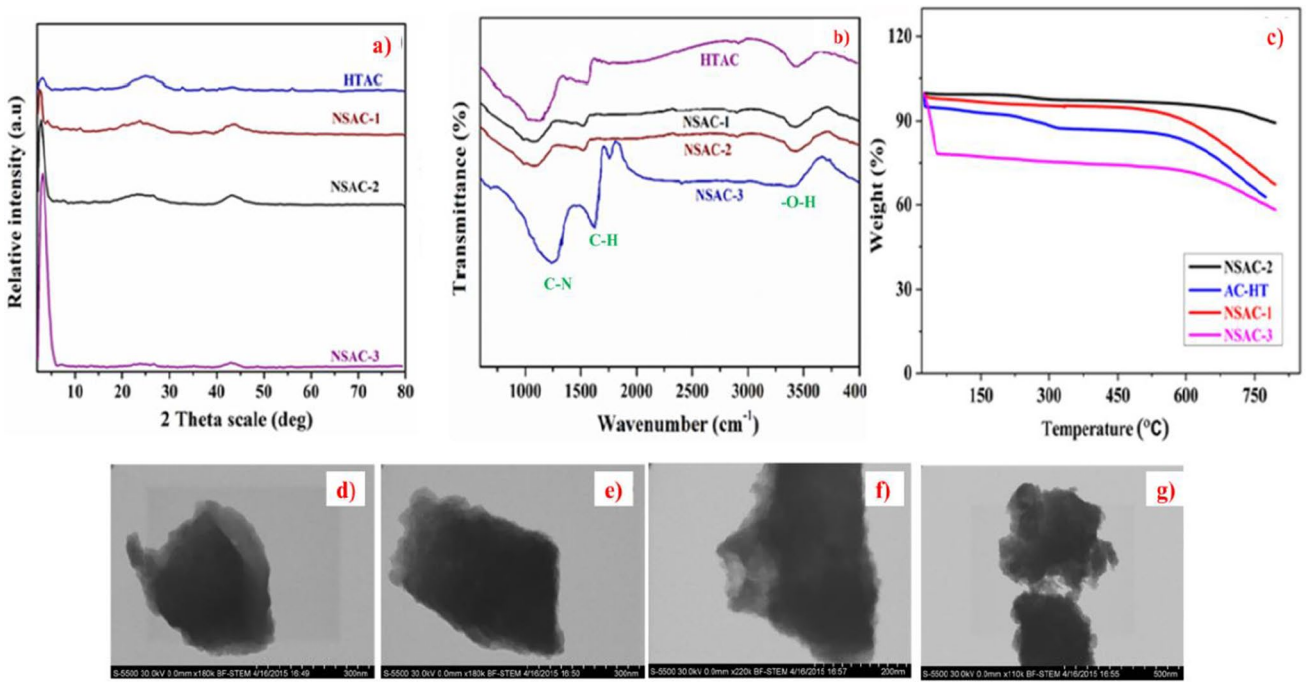

Fig. 2 (**a**) XRD, (**b**) FT-IR, (**c**) TGA profiles, and (**d**–**g**) TEM images of HTAC, NSAC-1, NSAC-2, and NSAC-3 samples

becomes stronger, possibly due to an increase in polarity in the carbon backbone. Therefore, the FT-IR analysis confirms that N-H, C-N, and S=O species exist in the carbon samples. In a nutshell, we have succeeded in co-doping nitrogen and sulfur in AC.

In order to study the thermal stability of all doped and undoped carbon samples, thermal gravimetric analysis (TGA) was carried out in an inert atmosphere (Fig. 2c). The TGA curves of NSAC-2 and NSAC-1 show more thermal stability compared to HTAC and NSAC-3 due to hetero atom doping. However, NSAC-3 is showing less thermal stability, which might be the destruction of the carbon sample and a sharp weight loss from 200 to 600 °C (Fig. 2c). During higher temperatures, the escape of H and O atoms leads to the removal of H_2O, CO_2, and CO which might be the reason behind such weight loss in NSAC-3. Transmission electron microscopy (TEM) images of carbon samples (Fig. 2d–g) show a laminar or plate-like structure which is the characteristic feature of activated carbon. A careful observation at the corners of nanostructures confirms the stacking of nanosheets. Many plate-like structures were overlapped or stacked over each other and had sizes around 200 to 300 nm. As per most of the previous reports, activated carbon produced by various methods demonstrated layered-like nanosheet morphology [23, 24]. Moreover, it is well known that such kind of nanostructure can bring out the high-specific surface area via large pore volume leading to huge space for infiltration of the electrolyte ions.

CV and GCD tests for HTAC, NSAC-1, NSAC-2, and NSAC-3 electrodes in symmetric coin cell device configuration were carried out to examine the impact of N and S heteroatoms on AC electrode material for supercapacitors. In Fig. 3a, cyclic voltammograms of these samples were displayed at 10 mV s^{-1}, and it shows nearly rectangular-like CV curves and high symmetry, demonstrating the electrode material's good capacitive performance, i.e., EDLC. The specific capacitance from a cyclic voltammogram (CV-Cs) concerning one electrode was calculated using the integration method with the help of IVMAN software using the formula: CV-Cs=$(Q\times 1000)(\Delta V\times m)^{-1}$, where Q is the total voltammetric charge storage, ΔV is the operating voltage range, and m is the mass of the active material in one electrode. The obtained specific capacitance values of HTAC, NSAC-1, NSAC-2, and NSAC-3 samples were 135 F g^{-1}, 274 F g^{-1}, 321 F g^{-1}, and 207 F g^{-1}, respectively. Among all the 4 samples, NSAC-2 is showing highest capacitance value (321 F g^{-1} at 10 mV s^{-1}). It can be seen that the NSAC-2 offers a superior specific capacitance. Additionally, CV curves of the optimized NSAC-2 were displayed in (Fig. 3b) at varied sweep rates, and it shows the voltammogram's slight departure from rectangular shape, suggesting that the pseudo capacitive process caused by the presence of heteroatoms is linked to the EDLC process. For NSAC-2 material, CV was recorded at various scan rates from 1 mV/s, 5 mV/s, 10 mV/s, 20 mV/s, 30 mV/s, 40 mV/s, 50 mV/s, and 100 mV/s, and their CV-Cs were found to be 366 F/g, 337 F/g, 321 F/g, 261 F/g, 242 F/g, 226 F/g, 213 F/g, and 165 F/g, respectively (Fig. 3b). The curves' forms are nearly rectangular and devoid of noticeable aberrations as intended. Additionally, the curves' shapes did not change as scan rates increased. This gadget is found to have high rates of charge and discharge in addition to having lower resistance to an analogous series.

Galvanostatic charge-discharge (GCD) experiment was carried out for the HTAC, NSAC-1, NSAC-2, and NSAC-3 samples in a two-electrode setup at various current densities, with the associated capacitance values displayed in Fig. 3c. Specific capacitance calculated from charging-discharging (CD-Cs) of the electrode material CD-Cs=$(2\times i\times \Delta t)(\Delta V\times m)^{-1}$, where I is the constant discharge current, Δt is the discharging time, ΔV is the operational voltage window, and m is the weight of the active material in one electrode. The obtained CD-Cs values of HTAC, NSAC-1, NSAC-2, and NSAC-3 samples were 142 F g^{-1}, 369 F g^{-1}, 417 F g^{-1}, and 277 F g^{-1}, respectively, at 0.7 A g^{-1}, wherein, among all the samples, NSAC-2 was superior. In order to poise the strong electronic attraction provided by the nitrogen and sulfur atoms, the carbon atoms obtain higher positive charge densities, which enhances the wettability of the nanocarbon (activated carbon) [25]. In the same manner, in our case, the addition of N and S to NSAC-1, NSAC-2, and NSAC-3 increases the wettability of the electrodes. Such a scenario provides strong interaction between electrolyte ions and doped AC electrode material as compared to HTAC. In other words, the higher wettability of NSAC-2 results in enhancement in the electrochemical performance originating due to higher surface activities (EDLC).

NSAC-2 electrode discharge curves at a current density of 0.7 A g^{-1}, 1.4 A g^{-1}, 3.5 A g^{-1}, and 5 A g^{-1} were shown in Fig. 3d (Table 1), which were lower in internal resistance (IR drop); thus, it was a sign of a good supercapacitor. With an increase in current density, the NSAC-2 CD-Cs diminish, which can be attributed to inadequate time to interrelate electrolyte ions with nanostructures [26, 27].

The specific capacitance was increased in CV-Cs and CD-Cs from HTAC to all NSAC samples because of the merger of N, S hetero atoms into the AC which leads to improvement in the overall conductivity and surface area. Figure 4 demonstrates the comparison of specific capacitance values from CV (CV-Cs) and GCD (CD-Cs) curves; both results are consistent in all samples. However, the comparison between all NSAC samples suggested that the specific capacitance was maximum for NSAC-2. Variation in the surface area is the main reason behind the discrepancy. The surface area was found to be increased from NSAC-1 to NSAC-2 and further decreased for NSAC-3,

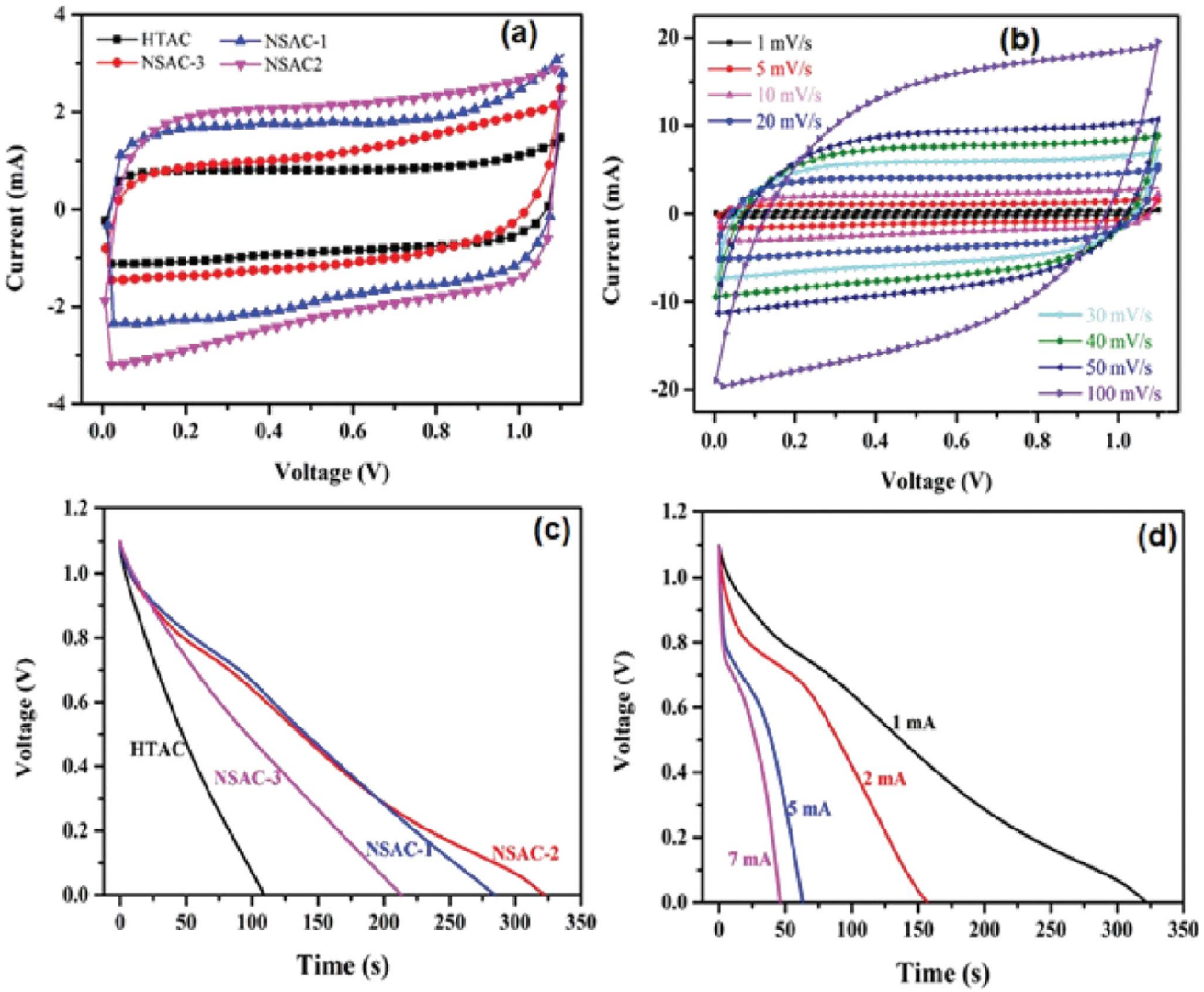

Fig. 3 Electrochemical features of all doped and undoped nanocarbon (activated carbon) samples (**a**) at a scan rate of 10 mV s^{-1}; CV curves of the HTAC, NSAC-1, NSAC-2, and NSAC-3 samples in 1 M H_2SO_4 solution. (**b**) CV curves at various sweep rates of the NSAC-2 in 1 M H_2SO_4 solution (**c**) at an applied current of 1mA; GCD curves of the HTAC, NSAC-1, NSAC-2, and NSAC-3 samples in 1 M H_2SO_4 solution and (d) GCD curves at various applied currents of the NSAC-2 in 1 M H_2SO_4 solution

whose values were mentioned in Supplementary Figs. S1 and S2 and Table S1. The large pore distribution and pore size of NSAC-2 provides higher electroactive sites for charge storage, resulting in superior electrochemical performance. The specific surface area of NSAC-3 was decreased because of the increased amount of thioacetamide which might destruct the carbon skeleton. With the increase in the N/S ratio, the mesoporosity content in the prepared sample increases, which, in turn, increases the specific capacitance as compared to the pristine activated sample. However, at the highest N/S ratio, i.e., NSAC-3, the surface area, pore size, and pore volume decrease than NSAC-2, which results in the reduction in electroactive sites. Finally, low capacitance resulted in NSAC-3 [28]. Generally, capacitive behavior improves with the specific surface area via enormous pore volume leading to huge space for infiltration of the electrolyte ions. NSAC-based symmetric coin cell supercapacitor

Table 1 CD-Cs, energy, and power density of NSAC-2 electrode material

Applied current (mA)	Current density (A g^{-1})	Capacitance (F g^{-1})	Energy density (W h Kg^{-1})	Power density (W Kg^{-1})
1	0.71	417	70	786
2	1.42	405	68	1571
5	3.5	390	65	3929
7	5	336	57	5500

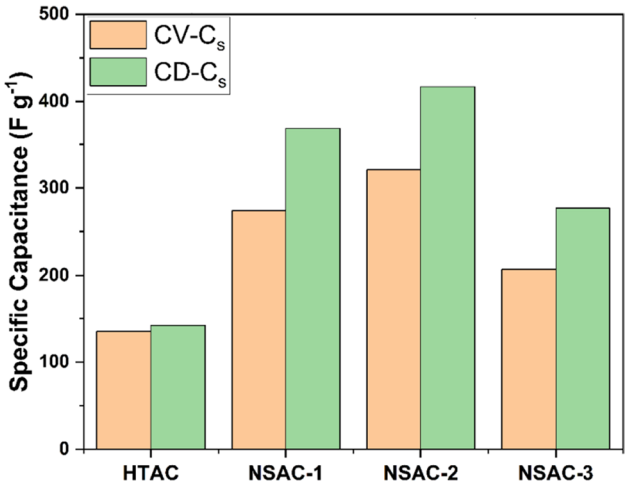

Fig. 4 Comparison between CV- and GCD-specific capacitance values of the HTAC, NSAC-1, NSAC-2, and NSAC-3 electrodes

device has the maximum energy density of 70 Wh kg^{-1} and the highest power density of 786 W kg^{-1}, as seen in the Ragone plots in Supplementary Fig. S3. The energy density may be kept at 57 Wh kg^{-1}, while the power density can be kept at 5500 W kg^{-1}. These values are comparable to those of a symmetric all-solid-state supercapacitor based on N,S-co-doped carbon nanofibers (16.35 Wh kg^{-1} at 147.15 W kg^{-1}) [29] and porous carbon generated from MOF (17.37 Wh kg^{-1} at 449.9 W kg^{-1}) [30] and greater than those of other heteroatom-doped porous carbon materials [29–36].

Furthermore, to check the device applicability of NSAC-2 of the CR2032 coin cell, the cyclic stability of the device was tested. The cycle stability of the NSAC-2 symmetric supercapacitor was illustrated in Fig. 5a. The capacitance decay is 20% within 100 cycles; after 200 charge/discharge cycles at a current density of 5 A g^{-1}, it was stabilized at 76% retention and that was maintained up to 60,000 cycles. The sudden decay within 200 cycles may be due to the peel-off of the active materials, as some particles were observed in the electrolyte solution [37].

The self-discharge study (SDS) is an important factor of supercapacitors for energy preservation [38]. The SDS patterns for the HTAC, NSAC-1, NSAC-2, and NSAC-3 electrodes were demonstrated in Fig. 5b. For the SDS, with a 2 mA current density, the device was charged up to 1.1 V (i.e., its operating voltage), and then, the open circuit voltage (OCV) of the device was measured by considering the function of time. The OCV of the NSAC-2 device reached 0.625 V (58.6% of the applied voltage is retained after 1 day), which indicates that the superior performance of NSAC-2 is better than the previously reported results [39–41]. NSAC-1 device reached 0.03 V, NSAC-3 device reached 0.003 V after 24 h, and AC device reached 0.001 V within 1 h, as shown in Fig. 6b.

The EIS analysis is further evidenced to study the mechanism of charge storage. The HTAC and NSAC samples' frequency-dependent behavior is tested from 40 kHz to 10 mHz at 0.7 V, and the resulting Nyquist plots are displayed in Fig. 6a. In the high-frequency range, it is made up of a single semicircle, while in the low-frequency region, it is made up of a vertical line. The comparable circuits are derived from the simulation of the experimental data using Zman software and are displayed as an inset in Fig. 6a. The semicircle occurs due to high frequency, which gives intercept on the real axis known as series resistance (R_s) information. For HTAC, NSAC-1, NSAC-2, and NSAC-3, the values of R_s are 0.11 Ω, 0.095 Ω, 0.079 Ω, and 0.068 Ω, respectively. The semicircle's diameter can be used to calculate the charge transfer resistance (R_{ct}), which is linked

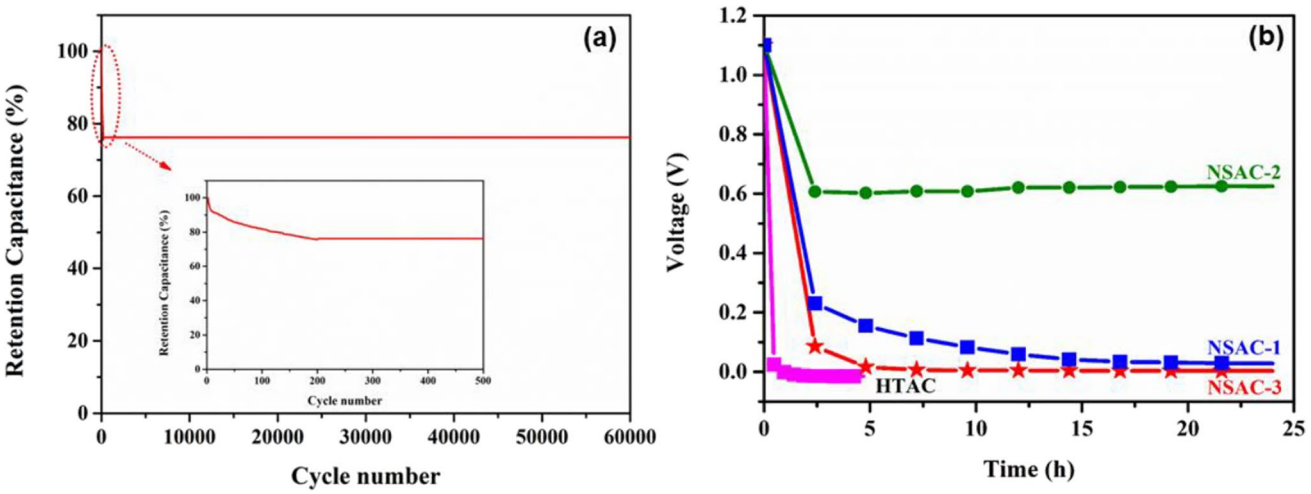

Fig. 5 (**a**) Cycle life diagram of NSAC-2 supercapacitor cell in solution (1 M H_2SO_4) measured at applied current density of 5 A g^{-1}. (**b**) Self-discharge curves of the HTAC, NSAC-1, NSAC-2, and NSAC-3 samples

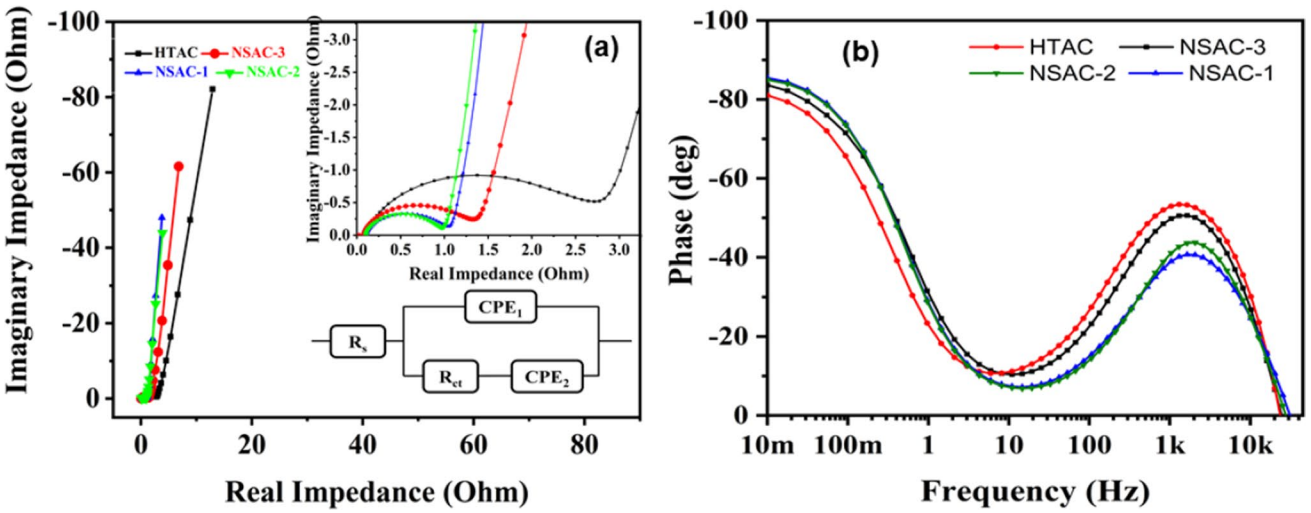

Fig. 6 (**a**) Nyquist plot (inset showing the circuit diagram) and (**b**) phase angle versus frequency of HTAC, NSAC-1, NSAC-2, and NSAC-3 electrodes (frequency 40 kHz–10 mHz at 0.7 V)

to the system's charge transfer barriers. The "ion transfer barrier" between the electrolyte and capacitive material as well as the "electron transfer barrier" between the capacitive material and the current collector are the barriers. The reduction in R_s and R_{ct} values revealed the increment in the overall conductivity of the electrode material. The doping in AC was confirmed by the aforementioned characterizations like XPS and FT-IR. Furthermore, its constructive effect on the enhancement of electrochemical activity was confirmed in this section. Due to variations in relaxation times, porosity, electrode type, and dynamic disorder, the presence of CPE1 and CPE2 (constant phase elements aroused due to double-layer capacitive and pseudocapacitive) suggests that the double-layer element exhibits less-than-ideal capacitor behavior. In the current study, values of CPE1 and CPE2 are discovered to be 2.14 F g^{-1}, 2.21 F g^{-1}, 2.14 F g^{-1} and 220 F g^{-1}, 425 F g^{-1}, 458 F g^{-1}, 309 F g^{-1} for HTAC, NSAC-1, NSAC-2, and NSAC-3 correspondingly, with corresponding "n" values of 0.70 and 0.93, 0.73 and 0.96, 0.76 and 0.96, and 0.76 and 0.94 (n =1 represents pure capacitive nature) for HTAC, NSAC-1, NSAC-2, and NSAC-3, respectively. From the results, we can say that both the constant phase elements of the carbon materials act similarly to capacitors. The time constant (t) of the carbon materials was calculated using the formula: $t = (2\pi f^*)^{-1}$. The time constant is determined from the maximum (midpoint) of the semicircle of the Nyquist plot and is found to be 1.48 ms, 1.18 ms, 0.75 ms, and 0.95 ms for HTAC, NSAC-1, NSAC-2, and NSAC-3, respectively. A lower time constant value means a faster charge-discharge phenomenon in the electrode materials [42–44]. When the semicircle transforms into a vertical line at a frequency known as knee frequency, the electrode's capacitive property will be leading. At frequencies higher than the knee frequency, the stored energy is partially inaccessible for any capacitive substance [45]. Simply, the frequency where the capacitive behavior starts in the Nyquist plot is the knee frequency. The knee frequency values for HTAC, NSAC-1, NSAC-2, and NSAC-3 are 5.93 Hz, 8.12 Hz, 11.0 Hz, and 4.27 Hz, respectively, indicating capacitive properties of NSAC-2 can be achieved at higher frequencies than NSAC-1, HTAC, and NSAC-3. Bode plots of carbon samples are shown in Fig. 6b. The phase angle values of HTAC, NSAC-1, NSAC-2, and NSAC-3 obtained from the bode diagram are 81°, 85°, 85°, and 84°, respectively, which are nearby to that of an ideal capacitor 90°. In a nutshell, nitrogen and sulfur co-doped AC expressively increased the surface activity and enhanced double-layer capacitance due to the conjugation between the π-system of the carbon framework and the lone-pair electrons of heteroatoms. The above statement is supported by the EIS studies, bode plot, and the increment in the specific capacitance values (as seen in CV and GCD).

4 Conclusion

In summary, we hydrothermally produced N, S-co-doped activated carbons. A coin cell device setup was used to examine the prepared samples for their electrochemical characteristics. The optimized sample of the symmetrical solid-state capacitor we made has a specific capacitance of 405 F g^{-1} at 1.4 A g^{-1} and an energy density of 68 Wh kg^{-1} and a power density of 1571 W kg^{-1}. Furthermore, even at 5 A g^{-1}, the activated carbon has an excellent long cycling life, losing only 24% of its opening capacitance after 60,000 cycles. High surface area, numerous micropores, porous

hierarchical structure, and high N and S content all contribute to the resulting material's good capacitive performance.

Supplementary Information The online version contains supplementary material available at https://doi.org/10.1007/s42247-023-00503-1.

Acknowledgements This work was supported by Qatar University through a National Capacity Building Program Grant (NCBP) [QUCP-CAM-20/23-463]. The publication of the article was funded by the Qatar National Library. Statements made herein are solely the responsibility of the authors.

Funding Open Access funding provided by the Qatar National Library.

Declarations

Conflict of interest The authors declare no competing interests.

References

1. A.Q. Al-Shetwi, Sustainable development of renewable energy integrated power sector: trends, environmental impacts, and recent challenges. Sci. Total Environ. **822**, 153645 (2022). https://doi.org/10.1016/j.scitotenv.2022.153645
2. C. Venkateswara Raju, C. Hwan Cho, G. Mohana Rani, et al., Emerging insights into the use of carbon-based nanomaterials for the electrochemical detection of heavy metal ions. Coord. Chem. Rev. **476**, 214920 (2023). https://doi.org/10.1016/j.ccr.2022.214920
3. R. Umapathi, C. Venkateswara Raju, S. Majid Ghoreishian, et al., Recent advances in the use of graphitic carbon nitride-based composites for the electrochemical detection of hazardous contaminants. Coord. Chem. Rev. **470**, 214708 (2022). https://doi.org/10.1016/j.ccr.2022.214708
4. R. Umapathi, S.M. Ghoreishian, S. Sonwal, et al., Portable electrochemical sensing methodologies for on-site detection of pesticide residues in fruits and vegetables. Coord. Chem. Rev. **453**, 214305 (2022). https://doi.org/10.1016/j.ccr.2021.214305
5. J. Liu, J. Wang, C. Xu, et al., Advanced energy storage devices: basic principles, analytical methods, and rational materials design. Adv. Sci. **5**, 1700322 (2018). https://doi.org/10.1002/advs.201700322
6. S. Rajagopal, R. Pulapparambil Vallikkattil, M. Mohamed Ibrahim, D.G. Velev, Electrode materials for supercapacitors in hybrid electric vehicles: challenges and current progress. Condens. Matter. **7**, 6 (2022). https://doi.org/10.3390/condmat7010006
7. M.A. Hannan, S.M. Abu, A.Q. Al-Shetwi, et al., Hydrogen energy storage integrated battery and supercapacitor based hybrid power system: a statistical analysis towards future research directions. Int. J. Hydrogen Energy. **47**, 39523–39548 (2022).https://doi.org/10.1016/j.ijhydene.2022.09.099
8. V. Ghai, K. Chatterjee, P.K. Agnihotri, Vertically aligned carbon nanotubes-coated aluminium foil as flexible supercapacitor electrode for high power applications. Carbon Lett. **31**, 473–481 (2021). https://doi.org/10.1007/s42823-020-00176-4
9. J. Cheng, Z. Lu, X. Zhao, et al., Electrochemical performance of porous carbons derived from needle coke with different textures for supercapacitor electrode materials. Carbon Lett. **31**, 57–65 (2021). https://doi.org/10.1007/s42823-020-00149-7
10. N. López-Salas, F. del Monte, A. Tamayo, et al., Sulfur-doped carbons prepared from eutectic mixtures containing hydroxymethylthiophene as metal-free oxygen reduction catalysts. Chem. Sus. Chem. **7**, 3347–3355 (2014). https://doi.org/10.1002/cssc.201402753
11. J.P. Paraknowitsch, A. Thomas, Doping carbons beyond nitrogen: an overview of advanced heteroatom doped carbons with boron, sulphur and phosphorus for energy applications. Energy. Environ. Sci. **6**, 2839–2855 (2013). https://doi.org/10.1039/C3EE41444B
12. E.N. Nxumalo, N.J. Coville, Nitrogen doped carbon nanotubes from organometallic compounds: a review. Materials **3**, 2141–2171 (2010). https://doi.org/10.3390/ma3032141
13. S. Zhang, M.S. Miran, A. Ikoma, et al., Protic ionic liquids and salts as versatile carbon precursors. J. Am. Chem. Soc. **136**, 1690–1693 (2014). https://doi.org/10.1021/ja411981c
14. A.G. El-Deen, M. El-Newehy, C.S. Kim, N.A.M. Barakat, Nitrogen-doped, FeNi alloy nanoparticle-decorated graphene as an efficient and stable electrode for electrochemical supercapacitors in acid medium. Nanoscale Res. Lett. **10**, 1–7 (2015). https://doi.org/10.1186/s11671-015-0778-6
15. C. Wang, Y. Zhou, L. Sun, et al., Sustainable synthesis of phosphorus- and nitrogen-co-doped porous carbons with tunable surface properties for supercapacitors. J. Power Sources **239**, 81–88 (2013). https://doi.org/10.1016/j.jpowsour.2013.03.126
16. S. Shaheen Shah, S.M. Abu Nayem, N. Sultana, et al., Preparation of sulfur-doped carbon for supercapacitor applications: a review. Chem. Sus. Chem. **15**, e202101282 (2022). https://doi.org/10.1002/cssc.202101282
17. M. Seredych, T.J. Bandosz, S-doped micro/mesoporous carbon–graphene composites as efficient supercapacitors in alkaline media. J. Mater. Chem. A. **1**, 11717–11727 (2013). https://doi.org/10.1039/C3TA12252B
18. R. Bolagam, R. Boddula, P. Srinivasan, One-step preparation of sulfonated carbon and subsequent preparation of hybrid material with polyaniline salt: a promising supercapacitor electrode material. J. Solid State Electrochem. **21**, 1313–1322 (2017). https://doi.org/10.1007/s10008-016-3487-x
19. R. Bolagam, R. Boddula, P. Srinivasan, Design and synthesis of ternary composite of polyaniline-sulfonated graphene oxide-TiO2 nanorods: a highly stable electrode material for supercapacitor. J. Solid State Electrochem. **22**, 129–139 (2018). https://doi.org/10.1007/s10008-017-3732-y
20. C. Hu, C. Yu, M. Li, et al., Nitrogen-doped carbon dots decorated on graphene: a novel all-carbon hybrid electrocatalyst for enhanced oxygen reduction reaction. Chem. Commun. **51**, 3419–3422 (2015). https://doi.org/10.1039/C4CC08735F
21. J. Wang, R. Ma, Z. Zhou, et al., Magnesiothermic synthesis of sulfur-doped graphene as an efficient metal-free electrocatalyst for oxygen reduction. Sci. Rep. **5** (2015). https://doi.org/10.1038/srep09304
22. X. An, G. Xing, J. Wang, et al., Preparation of activated carbon spheres and their electrochemical properties as supercapacitor electrode. Carbon Lett. **31**, 667–676 (2021). https://doi.org/10.1007/s42823-021-00241-6

23. X. Fan, C. Yu, J. Yang, et al., A layered-nanospace-confinement strategy for the synthesis of two-dimensional porous carbon nanosheets for high-rate performance supercapacitors. Adv. Energy. Mater. **5**, 1401761 (2015). https://doi.org/10.1002/aenm.201401761
24. V. Thirumal, R. Yuvakkumar, G. Ravi, et al., Characterization of activated biomass carbon from tea leaf for supercapacitor applications. Chemosphere **291**, 132931 (2022). https://doi.org/10.1016/j.chemosphere.2021.132931
25. D. Zhang, L. Zheng, Y. Ma, et al., Synthesis of nitrogen- and sulfur-codoped 3D cubic-ordered mesoporous carbon with superior performance in supercapacitors. ACS Appl. Mater. Interfaces **6**, 2657–2665 (2014). https://doi.org/10.1021/am405128j
26. M.A. Desai, A. Kulkarni, G. Gund, S.D. Sartale, SILAR grown K+ and Na+ ions preinserted MnO2 nanostructures for supercapacitor applications: a comparative study. Energy & Fuels **35**, 4577–4586 (2021). https://doi.org/10.1021/acs.energyfuels.0c04252
27. M.A. Desai, A.S. Vedpathak, A.R. Bhapkar, et al., An investigation of chemical and electrochemical conversion of SILAR grown Mn3O4 into MnO2 thin films. J. Environ. Manage. **299**, 113564 (2021). https://doi.org/10.1016/j.jenvman.2021.113564
28. S. Ahmed, A. Ahmed, M. Rafat, Nitrogen doped activated carbon from pea skin for high performance supercapacitor. Mater. Res. Express **5**, 045508 (2018). https://doi.org/10.1088/2053-1591/aabbe7
29. L. Chen, Z. Wen, L. Chen, et al., Nitrogen and sulfur co-doped porous carbon fibers film for flexible symmetric all-solid-state supercapacitors. Carbon N Y **158**, 456–464 (2020). https://doi.org/10.1016/j.carbon.2019.11.012
30. F. Yu, T. Wang, Z. Wen, H. Wang, High performance all-solid-state symmetric supercapacitor based on porous carbon made from a metal-organic framework compound. J. Power Sources **364**, 9–15 (2017). https://doi.org/10.1016/j.jpowsour.2017.08.013
31. H.-W. Chang, Y.-R. Lu, J.-L. Chen, et al., Electrochemically activated reduced graphene oxide used as solid-state symmetric supercapacitor: an X-ray absorption spectroscopic investigation. J. Phys. Chem. C **120**, 22134–22141 (2016). https://doi.org/10.1021/acs.jpcc.6b04936
32. Z. Song, D. Zhu, D. Xue, et al., Nitrogen-enriched hollow porous carbon nanospheres with tailored morphology and microstructure for all-solid-state symmetric supercapacitors. ACS Appl. Energy Mater. **1**, 4293–4303 (2018). https://doi.org/10.1021/acsaem.8b00928
33. W. Na, J. Jun, J.W. Park, et al., Highly porous carbon nanofibers co-doped with fluorine and nitrogen for outstanding supercapacitor performance. J. Mater. Chem. A Mater. **5**, 17379–17387 (2017). https://doi.org/10.1039/C7TA04406B
34. M. Chen, D. Yu, X. Zheng, X. Dong, Biomass based N-doped hierarchical porous carbon nanosheets for all-solid-state supercapacitors. J. Energy Storage **21**, 105–112 (2019). https://doi.org/10.1016/j.est.2018.11.017
35. X. Li, K. Liu, Z. Liu, et al., Hierarchical porous carbon from hazardous waste oily sludge for all-solid-state flexible supercapacitor. Electrochim. Acta. **240**, 43–52 (2017). https://doi.org/10.1016/j.electacta.2017.04.061
36. Y. Cheng, L. Huang, X. Xiao, et al., Flexible and cross-linked N-doped carbon nanofiber network for high performance freestanding supercapacitor electrode. Nano Energy **15**, 66–74 (2015). https://doi.org/10.1016/j.nanoen.2015.04.007
37. C. Tang, Z. Tang, H. Gong, Hierarchically porous Ni-Co oxide for high reversibility asymmetric full-cell supercapacitors. J. Electrochem. Soc. **159**, A651 (2012). https://doi.org/10.1149/2.074205jes
38. S. Hamedi, T. Ghanbari, Z. Hosseini, E. Moshksar, Self-discharge estimation of supercapacitor modules at different ventilation levels. J. Energy Storage **52**, 104822 (2022). https://doi.org/10.1016/j.est.2022.104822
39. C. Meng, C. Liu, L. Chen, et al., Highly flexible and all-solid-state paperlike polymer supercapacitors. Nano Lett. **10**, 4025–4031 (2010). https://doi.org/10.1021/nl1019672
40. L. Yuan, X.-H. Lu, X. Xiao, et al., Flexible solid-state supercapacitors based on carbon nanoparticles/MnO2 nanorods hybrid structure. ACS Nano **6**, 656–661 (2012). https://doi.org/10.1021/nn2041279
41. Y. Jin, H. Chen, M. Chen, et al., Graphene-patched CNT/MnO2 nanocomposite papers for the electrode of high-performance flexible asymmetric supercapacitors. ACS Appl. Mater. Interfaces **5**, 3408–3416 (2013). https://doi.org/10.1021/am400457x
42. S. Uppugalla, U. Male, P. Srinivasan, Design and synthesis of heteroatoms doped carbon/polyaniline hybrid material for high performance electrode in supercapacitor application. Electrochim. Acta **146**, 242–248 (2014). https://doi.org/10.1016/j.electacta.2014.09.047
43. S. Uppugalla, R. Boddula, P. Srinivasan, Methyl triphenylphosphonium permanganate as a novel oxidant for aniline to polyaniline-manganese(II, IV) oxide: material for high performance pseudocapacitor. J. Solid State Electrochem. **22**, 407–415 (2018). https://doi.org/10.1007/s10008-017-3770-5
44. B. Rajender, S. Palaniappan, Organic solvent soluble methyltriphenylphosphonium peroxodisulfate: a novel oxidant for the synthesis of polyaniline and the thus prepared polyaniline in high performance supercapacitors. New J. Chem. **39**, 5382–5388 (2015). https://doi.org/10.1039/C5NJ00979K
45. R. Bolagam, R. Boddula, P. Srinivasan, Synthesis of highly crystalline polyaniline with the use of (Cyclohexylamino)-1-propanesulfonic acid for supercapacitor. J. Appl. Electrochem. **45**, 51–56 (2015). https://doi.org/10.1007/s10800-014-0753-4